



Interlayer exchange coupling between layers with perpendicular and easy-plane magnetic anisotropies

Lorenzo Fallarino, Volker Sluka, Bartek Kardasz, Mustafa Pinarbasi, Andreas Berger, and Andrew D. Kent

Citation: [Applied Physics Letters](#) **109**, 082401 (2016); doi: 10.1063/1.4960795

View online: <http://dx.doi.org/10.1063/1.4960795>

View Table of Contents: <http://scitation.aip.org/content/aip/journal/apl/109/8?ver=pdfcov>

Published by the [AIP Publishing](#)

Articles you may be interested in

[Evolution of perpendicular magnetized tunnel junctions upon annealing](#)

Appl. Phys. Lett. **108**, 172409 (2016); 10.1063/1.4948378

[Ferromagnetic resonance of exchange-coupled perpendicularly magnetized bilayers](#)

J. Appl. Phys. **119**, 153905 (2016); 10.1063/1.4947227

[Joint perpendicular anisotropy and strong interlayer exchange coupling in systems with thin vanadium spacers](#)

J. Appl. Phys. **117**, 163911 (2015); 10.1063/1.4919089

[Interlayer exchange coupled composite free layer for CoFeB/MgO based perpendicular magnetic tunnel junctions](#)

J. Appl. Phys. **114**, 203901 (2013); 10.1063/1.4833252

[Interlayer exchange coupling between \[Pd/Co\] multilayers and CoFeB/MgO layers with perpendicular magnetic anisotropy](#)

Appl. Phys. Lett. **101**, 242403 (2012); 10.1063/1.4770300

The image shows the cover of an Applied Physics Reviews journal. It features a blue and orange color scheme with a molecular structure background. The text 'NEW Special Topic Sections' is prominently displayed in white. Below it, 'NOW ONLINE' is written in yellow, followed by the title 'Lithium Niobate Properties and Applications: Reviews of Emerging Trends' in white. The AIP Applied Physics Reviews logo is in the bottom right corner.

NEW Special Topic Sections

NOW ONLINE
Lithium Niobate Properties and Applications:
Reviews of Emerging Trends

AIP Applied Physics
Reviews

Interlayer exchange coupling between layers with perpendicular and easy-plane magnetic anisotropies

Lorenzo Fallarino,^{1,2} Volker Sluka,¹ Bartek Kardasz,³ Mustafa Pinarbasi,³ Andreas Berger,² and Andrew D. Kent¹

¹Department of Physics, New York University, New York, New York 10003, USA

²CIC nanoGUNE Consolider, 20018 Donostia-San Sebastian, Spain

³Spin Transfer Technologies, Inc., Fremont, California 94538, USA

(Received 24 June 2016; accepted 30 July 2016; published online 22 August 2016)

Interlayer exchange coupling between layers with perpendicular and easy-plane magnetic anisotropies separated by a non-magnetic spacer is studied using ferromagnetic resonance. The samples consist of a Co/Ni multilayer with perpendicular magnetic anisotropy and a CoFeB layer with easy-plane anisotropy separated by a variable thickness Ru layer. At a fixed frequency, we show that there is an avoided crossing of layer ferromagnetic resonance modes providing direct evidence for interlayer coupling. The mode dispersions for different Ru thicknesses are fit to a Heisenberg-type model to determine the interlayer exchange coupling strength and layer properties. The resulting interlayer exchange coupling varies continuously from antiferromagnetic to ferromagnetic as a function of the Ru interlayer thickness. These results show that the magnetic layer single domain ground state consists of magnetizations that can be significantly canted with respect to the layer planes and the canting can be tuned by varying the Ru thickness and the layer magnetic characteristics, a capability of interest for applications in spin-transfer torque devices. *Published by AIP Publishing.* [<http://dx.doi.org/10.1063/1.4960795>]

Artificially layered magnetic systems display a remarkable variety of new physical phenomena, with important technological applications in information processing and storage.^{1–4} Magnetic order in these structures can be strongly influenced by the layer properties and interlayer exchange coupling (IEC).^{5–8} The latter's sign and strength can be controlled by inserting a non-magnetic spacer between ferromagnetic layers. By changing the thickness of the spacer, the interlayer coupling can be varied between antiferromagnetic and ferromagnetic.^{9–15} However, in most cases, samples studied to date have individual ferromagnetic layers that have collinear easy magnetic axis (either perpendicular or in the layer plane), leading to either ferromagnetic or antiferromagnetic ground states of the coupled layers.

At the same time, the intense study of spin-current driven magnetization reversal has led to the discovery of new possibilities for high-performance non-volatile memory technology such as spin-transfer torque (STT) based devices.¹⁶ The application of these technologies still faces many challenges, including ultrafast manipulation of the magnetization, reduction of the switching current, and increase of thermal stability. Through the introduction of materials with perpendicular magnetic anisotropy (PMA), it has been possible to increase the switching speed and the thermal stability as well as to reduce the switching current.^{17–20} In magnetic tunnel junctions (MTJ), one possible structure that supports an overall perpendicular configuration is the PMA/nonmagnetic (NM)/CoFeB layer stack, where the PMA and the CoFeB layers are strongly exchange coupled through the NM spacer.^{21,22} However, when all the magnetic layers have a perpendicular easy axis, the STT vanishes due to the collinear magnetization configuration. One possible solution is the introduction of a magnetic layer (either a fixed or free

magnetic layer in a STT device) with an easy axis canted with respect to the perpendicular direction. In doing this, the STT would be present when a current is first applied, and moreover, thermal fluctuations would not be needed to initiate STT magnetization switching.^{23,24}

In this letter, we report the properties of layers with perpendicular and easy plane magnetic anisotropies and strong IEC to determine their single domain magnetic ground states as a function of the coupling strength and sign. Instead of the MTJ structures mentioned above in which the (PMA and CoFeB) magnetic layers are strongly ferromagnetically coupled, we developed and studied a model material system with non-collinear magnetization and variable IEC: a Co/Ni (CoNi) multilayer with PMA and a Co₆₀Fe₂₀B₂₀ (CoFeB) layer with in-plane magnetic anisotropy separated by a variable thickness Ru interlayer. We use vector network analyzer ferromagnetic resonance spectroscopy (VNA-FMR) to determine the coupled dynamic modes of these layers,^{25–27} measuring their dispersion as a function of the applied magnetic field.

We fabricated the following bi-magnetic layer stacks on oxidized silicon wafers by dc magnetron sputtering: Ta(5)/Cu(3)/Ni(0.65)/Co(0.3)/[Ni(0.6)/Co(0.2)]₅/Co(0.18)/Ru(t_{Ru})/CoFeB(3)/Ta(3).²⁸ The thickness of the Ru spacer (t_{Ru}) was varied between 0.71 and 1.17 nm across the full 150 mm diameter of the wafer (i.e., there is a Ru thickness gradient of 3 pm/mm). A schematic of the sample is shown in Fig. 1. The wafer was diced into 8 × 8 mm² pieces, leading to 18 samples with different average Ru thicknesses. In addition to this sample, we prepared both a sample containing just the CoFeB layer, specifically Ta(5)/Cu(3)/Ru(1)/CoFeB(3)/Ta(3),²⁸ and a stack containing just the PMA layer, Ta(5)/Cu(3)/Ni(0.65)/Co(0.3)/[Ni(0.6)/Co(0.2)]₅/Co(0.18)/Ru(3).²⁸ We analyzed these single layer samples with FMR and vibrating sample

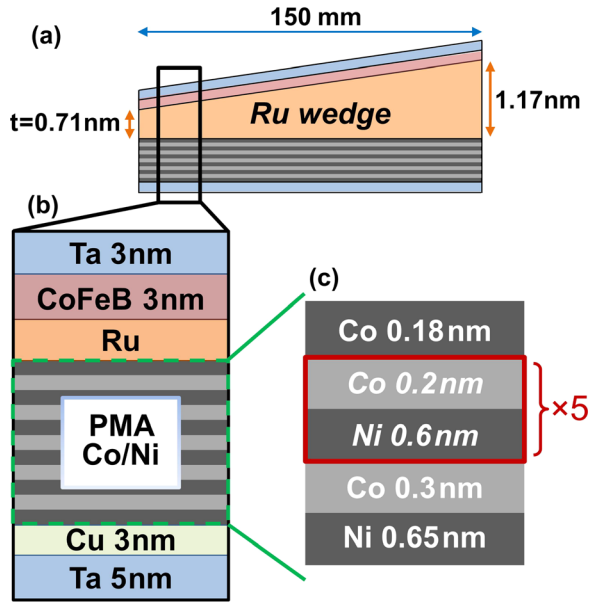


FIG. 1. (a) Schematic of the wedge sample studied in this work. (b) Detailed layer structure. (c) Co/Ni multilayer structure with strong perpendicular magnetic anisotropy.

magnetometry (VSM), in order to measure the moment density and gyromagnetic ratio of the two materials. For CoFeB and CoNi, we obtained a moment density of 1.345×10^6 A/m ($\mu_0 M_s = 1.690$ T) and 4.775×10^5 A/m ($\mu_0 M_s = 0.600$ T), respectively. The corresponding gyromagnetic ratios were 2.19×10^5 m/(As) for CoFeB and 2.28×10^5 m/(As) for CoNi. The effective PMA (i.e., the uniaxial out-of-plane anisotropy minus the demagnetization term, see below) of the CoNi single layer sample was determined to be 0.400 T by measuring in-plane FMR and VSM-magnetometry data. We also found that in addition to the demagnetizing term, the CoFeB single layer film exhibits an easy-plane anisotropy of about 0.210 T, which produces a hard axis saturation field of 1.9 T, greater than $\mu_0 M_s$. Such an additional easy axis type anisotropy has been reported previously for CoFeB/Ru layers.^{29,30}

Each individual film FMR mode can be thought of as one of two eigenmodes of a hypothetical two-layer system, with the interlayer exchange coupling switched off. These two independent modes are represented as green triangles (CoNi) and black squares (CoFeB) in Fig. 2(a), which shows the resonance field of each mode as a function of the out-of-plane angle of the applied field θ . The excitation frequency was fixed at 25 GHz. We show the measurement of a bi-magnetic layer sample with a Ru thickness of 1.05 nm³¹ displayed as blue circles. The corresponding microwave absorption lines are displayed in Fig. 2(b), with each measurement scan scaled to have the same amplitude and then offset by a constant value to permit comparison. One important difference between the two sets of measurements in Fig. 2(a), is the appearance of an avoided crossing (i.e., a frequency gap) between the two mode branches, indicated by the red arrow, roughly at the angle where the individual layers' modes cross. The avoided crossing is direct evidence for an interaction between the magnetic layers. Its angular shift with respect to the crossing of the two independent

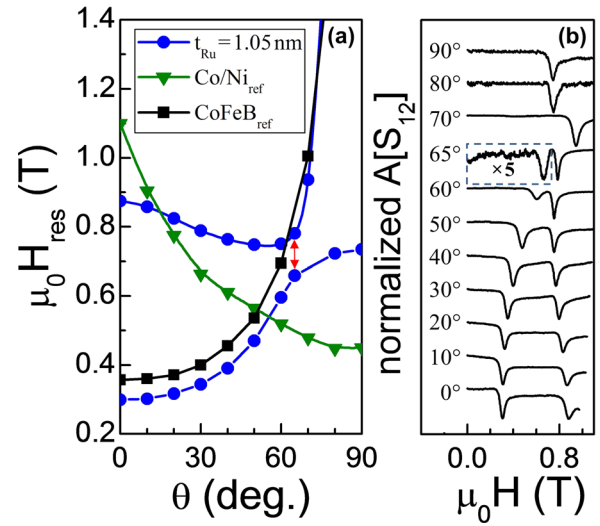


FIG. 2. (a) FMR resonant fields at 25 GHz as a function of the applied field angle relative to the sample plane ($\theta = 0$ is field in the sample plane). The green triangles are data for the Co/Ni reference sample, the black squares refers to a CoFeB reference sample and the blue circles indicate the data of the bi-magnetic layer sample with a 1.05 nm thick Ru layer. The solid lines are simply guides to the eye. (b) Corresponding normalized microwave absorption lines (amplitude of the S_{12} parameter) displayed as a function of the applied field angle. Within the dashed blue rectangle, the amplitude of the absorption signal has been multiplied by five to make the lower field absorption peak more visible. S_{12} is a component of the S-matrix that characterizes the microwave transmission of the coplanar waveguide, the ratio of the outgoing to incoming microwave signal.³² It was measured with a vector network analyzer at a fixed frequency while sweeping the applied magnetic field.

modes can be associated with changes in the magnetic anisotropy of the layers in the bi-magnetic layer samples (see the [supplementary material](#)).

In order to quantitatively determine the interaction strength, we performed FMR measurements with the field applied parallel to the sample plane. For each of the 18 coupled bi-magnetic layer samples, we measured the resonance field as a function of the applied RF field frequency, as shown in Fig. 3. We then model these data with an areal energy density that assumes a Heisenberg-type exchange coupling between the layers

$$\sigma_E(\mathbf{m}_1, \mathbf{m}_2) = -\mu_0 M_{s1} d_1 \mathbf{H} \cdot \mathbf{m}_1 - \frac{1}{2} \mu_0 M_{s1} d_1 H_{k1} m_{1z}^2 - J \mathbf{m}_1 \cdot \mathbf{m}_2 - \mu_0 M_{s2} d_2 \mathbf{H} \cdot \mathbf{m}_2 - \frac{1}{2} \mu_0 M_{s2} d_2 H_{k2} m_{2z}^2, \quad (1)$$

where the unit vectors $\mathbf{m}_i = (m_{ix}, m_{iy}, m_{iz})^T$ denote the layer magnetizations, with $i=1$ for the CoNi and $i=2$ for the CoFeB layer. Accordingly, M_{si} refers to the individual layers' saturation magnetizations. The terms involving the external magnetic field \mathbf{H} represent the Zeeman energy, and the expressions proportional to m_{iz}^2 are the effective anisotropy energy terms for the two layers. Here, $H_{k1} = H_{k1}^{(0)} - M_{s1} > 0$ is the effective perpendicular magnetic anisotropy of the CoNi multilayer, that is, the intrinsic anisotropy $H_{k1}^{(0)}$ minus the multilayer's saturation magnetization. To include anisotropy in the CoFeB layer, we add an internal field $H_{k2}^{(0)}$ as a modification to the demagnetizing field and accordingly define $H_{k2} = H_{k2}^{(0)} - M_{s2}$. The interlayer exchange coupling is J , with $J > 0$ corresponding to ferromagnetic coupling. μ_0 and d_i are the

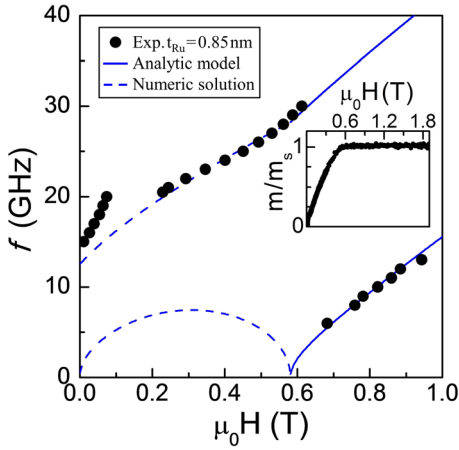


FIG. 3. Optic and acoustic FMR mode frequencies of a PMA-CoNi/Ru 0.85 nm/CoFeB structure as a function of the in-plane external magnetic field, displayed as black filled circles. These frequencies are obtained by fitting the modulus of the transmission coefficient S_{12} measured by VNA-FMR to a Lorentzian function. The solid blue lines represent the fit to the experimental data using solutions to Eq. (5) whereas the dashed blue lines are the continuation for the two frequencies branches below the saturation field, calculated using the parameters obtained from the fit above the saturation field. The inset shows the VSM hysteresis loop, normalized magnetic moment versus external in-plane field for the same sample.

magnetic permeability and the layer thicknesses, respectively. We fix the lab coordinate system by defining the projection of the external field \mathbf{H} in plane of the sample to coincide with the x -axis, and the out-of-plane projection of \mathbf{H} to be identified with the z -axis. With this energy density, the equation of motion for the magnetization of each layer is

$$\frac{d\mathbf{m}_i}{dt} = -\gamma_i \mathbf{m}_i \times \mathbf{H}_i(\mathbf{m}_1, \mathbf{m}_2), \quad (2)$$

where the layer-resolved effective fields $\mathbf{H}_i = -\frac{1}{\mu_0 M_{si} d_i} \nabla_{\mathbf{m}_i} \sigma_E$ are functions of both layer magnetizations, due to their interaction. In an external field, the bi-magnetic layer system will reside in a field-dependent ground state, a stationary solution of Eq. (2). In order to investigate the ferromagnetic resonance, we expand the equation of motion around the field-dependent ground state and study the small-angle excitations. For the expansion, in each layer, we switch to a rotated frame, where the new x -axis coincides with the ground state. Since the ground state in each case will lie in the x - z -plane of the original frame, the new frame is fixed by requiring that the new and original y -axes coincide. Denoting the coordinate tuples in the new frame by $\tilde{\mathbf{m}}_i$, in each layer, the new coordinates are related to the original ones by

$$\mathbf{m}_i = \begin{pmatrix} \cos \beta_i & 0 & -\sin \beta_i \\ 0 & 1 & 0 \\ \sin \beta_i & 0 & \cos \beta_i \end{pmatrix} \tilde{\mathbf{m}}_i =: R_i \tilde{\mathbf{m}}_i, \quad (3)$$

where β_i represents the out-of-plane angle of each individual layer magnetization. Thus, the system of equation of motion in the rotated frame reads

$$\frac{d\tilde{\mathbf{m}}_i}{dt} = -\gamma_i \tilde{\mathbf{m}}_i \times R_i^{-1} \mathbf{H}_i(R_1 \tilde{\mathbf{m}}_1, R_2 \tilde{\mathbf{m}}_2). \quad (4)$$

Expanding to first order in the four degrees of freedom of the magnetization and subsequent Fourier transformation leads to the eigenvalue problem

$$(-i\omega \mathbb{1} + \Gamma \mathfrak{A}) \delta \tilde{\mathbf{m}}(\omega) = 0, \quad (5)$$

where Γ contains the individual layers' gyromagnetic ratios and \mathfrak{A} is a four by four matrix that depends on the magnetic properties and the state around which the expansion is made, in this case, the applied field-dependent ground state (see the [supplementary material](#) for details).

In order to compute the eigenvalues of $\Gamma \mathfrak{A}$, the angles β_i characterizing the field-dependent ground state have to be known. Above the in-plane saturation field, $\beta_i = 0$, we obtain an analytic expression for each FMR mode frequency as a function of the system parameters and the external field (see Eqs. (S6) and (S7) in the [supplementary material](#)). The experimental data show that in addition to the changes induced by the interlayer exchange coupling, the individual-layer properties of the two subsystems are altered when they are "brought together" in the bi-magnetic layer samples. As described in detail in the [supplementary material](#), these changes in the magnetic layer properties are evidenced by the fact that although for certain Ru thicknesses, either one or the other of the two frequency branches comes close to its single layer film counterpart, there exists no Ru thickness value for which both frequency-versus-field dependencies simultaneously match those of the single layer samples.

In fact, by combining the two layers, the growth sequence and the overall electronic structure of the individual layers are modified, given that the electronic wave functions in this metallic structure extend throughout the layer stack, which is the origin of interlayer coupling in the first place. Additionally, changes in the thickness of the Ru spacer may introduce structural changes in the CoFeB layer. Thus, other materials properties, such as the magnetic anisotropy, may be expected to change in the multilayer structure as well. In order to incorporate changes in magnetic anisotropies on one hand, while at the same time keeping the number of free parameters to a minimum, we take the following approach: in addition to J , we let H_{k1} , the effective perpendicular anisotropy of the CoNi multilayer, be a fitting parameter. Regarding the CoFeB layer, we make the assumption that for high Ru thickness, $\mu_0 H_{k2}^{(0)}$ approaches the value found in the single layer CoFeB system. Therefore, in our fits, we let $\mu_0 H_{k2}^{(0)}$ interpolate linearly between zero at the low thickness end of the Ru wedge, and -210 mT on the high thickness end of the Ru wedge. To further reduce the number of free parameters for the fit, we fix the γ_i and M_{si} to the respective values obtained for the single layers.

One of the resulting fits of Eqs. (S6) and (S7) is shown in Fig. 3 as blue solid lines. The dashed blue lines are the continuation of the two frequency branches below the saturation field, where, prior to solving the eigenvalue problem, we obtain the field-dependent ground state by numerically solving Eq. (4) for the corresponding stationary point. In doing this, we use the parameters obtained by the fit above the saturation point, so that these numeric data provide a consistency check of the model and parameters in the vicinity of the

saturation field. At even lower fields, the layer magnetizations break up into domains, imposing a limit to the applicability of our macrospin model. We note that over the full range of Ru thicknesses studied we obtain fits of similar quality to the FMR spectra. Figure 4(b) displays the resulting coupling strength as a function of the t_{Ru} . For small Ru thickness, we find antiferromagnetic coupling which at $t_{\text{Ru}} \approx 1$ nm changes sign indicating ferromagnetic coupling. This behavior of J as a function of the Ru thickness is similar to that reported in Ref. 10, where collinear fcc Co multilayers coupled by Ru were investigated; we find an interlayer exchange coupling for 0.85 nm thick Ru that is half that of Ref. 10. Of course, quantitative agreement is not expected, as the interlayer coupling depends on many factors, including the composition and structure of the ferromagnets.¹³

From the fit parameters, we computed the zero-field ground state configuration for a corresponding single domain element, which we display as pictograms at discrete Ru thicknesses in Fig. 4(b). The zero-field polar angle of each layer magnetization as a function of the interlayer thickness is shown in panel (a). In the antiferromagnetic regime, the interlayer exchange coupling can result in significant tilting angles of the CoNi magnetic layer, whereas the CoFeB magnetization is more restricted to the sample plane, due to its larger effective anisotropy. Increasing the Ru thickness renders the IEC increasingly ferromagnetic, so that the mutual angle of the layer magnetizations in the ground state configuration decreases until both layers are essentially parallel and magnetized in-plane.

These results show that IEC can be harnessed to engineer tilted ground states in bilayer magnetic systems consisting of in-plane and out-of-plane magnetized materials, commonly used in spin-transfer device studies. Of course, in

extended films, the magnetic ground states will be multi-domain configurations. But when these layers are patterned into nanopillars (<100 nm diameter elements), as required for STT devices, we expect they will have the single domain ground states illustrated in Fig. 4. Further, there will be dipolar interactions between the magnetic layers in the patterned elements that we have not considered in this analysis. Moreover, we have found an extended Ru-thickness range, from 0.7 to 0.9 nm, in which the coupling strength and thus the layer magnetization orientations exhibit a rather weak dependence on t_{Ru} , which can make device properties less sensitive to variations in interlayer thickness.

In summary, we have investigated the interlayer exchange coupling in a sample consisting of PMA and easy-plane anisotropy magnetic layers. Using ferromagnetic resonance spectroscopy, we determined the IEC strength as a function of the Ru spacer thickness. For Ru thicknesses ranging from 0.7 nm to about 1 nm, strong antiferromagnetic coupling is observed, which leads to a canted single domain ground state. The mutual angles range from 120° in the antiferromagnetic regime down to 0° when the layers are coupled ferromagnetically at thicknesses around 1.17 nm. We note that since the IEC-induced effective fields acting on the individual layers are proportional to $J/(d_i M_{si})$, the saturation magnetizations and layer thicknesses could be used as additional means to vary the zero-field canting angle. We expect that when patterned into small elements, such bilayers could be utilized in spin-torque devices, such as memory cells or spin-torque oscillators, where the tilted ground state may reduce the influence of thermal noise on switching found in devices with collinear ground states and thus lead to both faster and more reliable magnetization switching.

See [supplementary material](#) for a description of our model of the ferromagnetic resonance spectra and further details about the analysis.

We thank Dr. Jonathan Sun for helpful discussions of this project. L.F. and A.B. acknowledge support from Basque Government under the Project No. PI2015_1_19 and from the Spanish Ministry of economy and competitiveness under the Project No. FIS2015-64519-R (MINECO/FEDER). L.F. acknowledges support from the Predoctoral Program of the Basque Government through the Grant No. PRE_2015_2_0126 and from the Pre-doctoral Mobility Program of the Basque Government under the Grant No. EP2015-1-14. This research was supported by Spin Transfer Technologies, Inc. and in part by National Science Foundation under Grant Nos. DMR-1309202 and DMR-1610416. A.D.K. also acknowledges support from the Institute for Nanoelectronics Discovery and Exploration (INDEX), a funded center of the Nanoelectronics Research Initiative (NRI), a Semiconductor Research Corporation (SRC) program sponsored by National Science Foundation's Engineering Research Centers (NERC) and the National Institute of Standards and Technology (NIST).

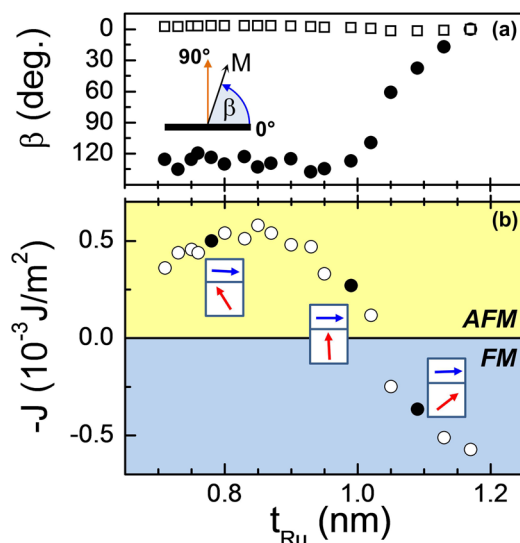


FIG. 4. (a) The single domain ground state magnetization canting angle β plotted as a function of the thickness of the Ru spacer layer. $\beta = 0$ corresponds to in-plane orientation of the magnetization. The open squares correspond to the CoFeB layer, whereas the filled circles correspond to the Co/Ni multilayers. (b) Interlayer exchange coupling J as a function of the Ru thickness. The insets illustrate remanent magnetic configurations of CoFeB/Ru/[Co/Ni]₅ for three different Ru thicknesses corresponding to the closest filled black circles. The CoFeB magnetization is illustrated with a blue arrow and the CoNi with a red arrow.

¹A. Fert, P. Grünberg, A. Barthélémy, F. Petroff, and W. Zinn, *J. Magn. Magn. Mater.* **140–144**, 1 (1995).

²I. Zutic, J. Fabian, and S. Das Sarma, *Rev. Mod. Phys.* **76**, 323 (2004).

- ³A. Hashimoto, S. Saito, K. Omori, H. Takashima, T. Ueno, and M. Takahashi, *Appl. Phys. Lett.* **89**, 032511 (2006).
- ⁴A. Berger, N. Supper, Y. Ikeda, B. Lengersfeld, A. Moser, and E. E. Fullerton, *Appl. Phys. Lett.* **93**, 122502 (2008).
- ⁵*Ultrathin Magnetic Structures III*, edited by M. D. Stiles, J. A. C. Bland, and B. Heinrich (Springer, 2005), pp. 99–142.
- ⁶P. Grünberg and D. E. Bürgler, *Handbook of Spintronics* (Springer, 2016), pp. 107–126.
- ⁷A. Ney, F. Wilhelm, M. Farle, P. Pouloupoulos, P. Srivastava, and K. Baberschke, *Phys. Rev. B* **59**, R3938 (1999).
- ⁸S. S. Kalarickal, X. Y. Xu, K. Lenz, W. Kuch, and K. Baberschke, *Phys. Rev. B* **75**, 224429 (2007).
- ⁹J. Fassbender, F. C. Nörtemann, R. L. Stamps, R. E. Camley, B. Hillebrands, G. Güntherodt, and S. S. P. Parkin, *J. Appl. Phys.* **73**, 5986 (1993).
- ¹⁰P. J. H. Bloemen, H. W. van Kesteren, H. J. M. Swagten, and W. J. M. de Jonge, *Phys. Rev. B* **50**, 13505 (1994).
- ¹¹S. S. P. Parkin, N. More, and K. P. Roche, *Phys. Rev. Lett.* **64**, 2304 (1990).
- ¹²G. Binash, P. Grünberg, F. Saurenbach, and W. Zinn, *Phys. Rev. B* **39**, 4828(R) (1989).
- ¹³S. S. Parkin, *Phys. Rev. Lett.* **67**, 3598 (1991).
- ¹⁴J. L. Leal and M. H. Kryder, *J. Appl. Phys.* **83**, 3720 (1998).
- ¹⁵A. Fernández-Pacheco, F. C. Ummelen, R. Mansell, D. Petit, J. H. Lee, H. J. M. Swagten, and R. P. Cowburn, *Appl. Phys. Lett.* **105**, 092408 (2014).
- ¹⁶A. V. Khvalkovskiy, D. Apalkov, S. Watts, R. Chepulska, R. S. Beach, A. Ong, X. Tang, A. Driskill-Smith, W. H. Butler, P. B. Visscher, D. Lottis, E. Chen, V. Nikitin, and M. Krounbi, *J. Phys. D: Appl. Phys.* **46**, 074001 (2013).
- ¹⁷A. D. Kent, B. Ozyilmaz, and E. del Barco, *Appl. Phys. Lett.* **84**, 3897 (2004).
- ¹⁸S. Mangin, D. Ravelosona, J. A. Katine, M. J. Carey, B. D. Terris, and E. E. Fullerton, *Nat. Mater.* **5**, 210 (2006).
- ¹⁹S. Ikeda, K. Miura, H. Yamamoto, K. Mizunuma, H. D. Gan, M. Endo, S. Kanai, J. Hayakawa, F. Matsukura, and H. Ohno, *Nat. Mater.* **9**, 721 (2010).
- ²⁰D. C. Worledge, G. Hu, D. W. Abraham, J. Z. Sun, P. L. Trouilloud, J. Nowak, S. Brown, M. C. Gaidis, E. J. O'Sullivan, and R. P. Robertazzi, *Appl. Phys. Lett.* **98**, 022501 (2011).
- ²¹M. Gottwald, J. J. Kan, K. Lee, S. H. Kang, and E. E. Fullerton, *APL Mater.* **1**, 022102 (2013).
- ²²T. Devolder, A. Le Goff, S. Eimer, and J. P. Adam, *J. Appl. Phys.* **117**, 163911 (2015).
- ²³H. Liu, D. Bedau, J. Z. Sun, S. Mangin, E. E. Fullerton, J. A. Katine, and A. D. Kent, *J. Magn. Magn. Mater.* **358–359**, 233–258 (2014).
- ²⁴T. N. Anh Nguyen, Y. Fang, V. Fallahi, N. Benatmane, S. M. Mohseni, R. K. Dumas, and J. Åkerman, *Appl. Phys. Lett.* **98**, 172502 (2011).
- ²⁵J. R. Fermin, M. A. Lucena, A. Azevedo, F. M. de Aguiar, and S. M. Rezende, *J. Appl. Phys.* **87**, 6421 (2000).
- ²⁶J. M. L. Beaujour, W. Chen, K. Krycka, C. C. Kao, J. Z. Sun, and A. D. Kent, *Eur. Phys. J. B* **59**, 475 (2007).
- ²⁷J. M. L. Beaujour, A. D. Kent, D. Ravelosona, I. Tudosa, and E. E. Fullerton, *J. Appl. Phys.* **109**, 033917 (2011).
- ²⁸All the layer thicknesses are given in nm.
- ²⁹Z. Wen, H. Sukegawa, T. Furubayashi, J. Koo, K. Inomata, S. Mitani, J. P. Hadorn, T. Ohkubo, and K. Hono, *Adv. Mater.* **26**, 6483 (2014).
- ³⁰Y. Liu, J. Zhang, S. Wang, S. Jiang, Q. Liu, X. Li, Z. Wu, and G. Yu, *ACS Appl. Mater. Interfaces* **7**, 26643–26648 (2015).
- ³¹Each $8 \times 8 \text{ mm}^2$ piece was cleaved into $2 \times 2 \text{ mm}^2$ pieces before measurement, and the central line of the FMR coplanar waveguide spans the width of one small piece (i.e. its 2 mm length). The main source of uncertainty in the Ru thickness is the selection of the piece after cleaving, about 0.02 nm.
- ³²Y. Ding, T. J. Klemmer, and T. M. Crawford, *J. Appl. Phys.* **96**, 2969 (2004).